OPEN ACCESS
CellPress

Cell Reports
Article

Invadopodia Are Required for Cancer Cell Extravasation and Are a Therapeutic Target for Metastasis

Hon S. Leong,[1] Amy E. Robertson,[1] Konstantin Stoletov,[3] Sean J. Leith,[1] Curtis A. Chin,[1] Andrew E. Chien,[1] M. Nicole Hague,[2] Amber Ablack,[1] Katia Carmine-Simmen,[3] Victor A. McPherson,[1] Carl O. Postenka,[2] Eva A. Turley,[2,4] Sara A. Courtneidge,[5] Ann F. Chambers,[2] and John D. Lewis[3,*]

[1]Translational Prostate Cancer Research Group, London Regional Cancer Program, 790 Commissioners Road East, London ON N6A 4L6, Canada
[2]London Regional Cancer Program, Cancer Research Laboratory Program, 790 Commissioners Road East, London ON N6A 4L6, Canada
[3]Department of Oncology, University of Alberta, 5-142C Katz Group Building, Edmonton AB T6G 2E1, Canada
[4]Departments of Biochemistry, Oncology, and Surgery, Western University, London, ON N6A 5C1, Canada
[5]Department of Cell, Developmental and Cancer Biology, Oregon Health & Science University, Collaborative Life Sciences Building, 2750 SW Moody Avenue, Portland, OR 97239, USA
*Correspondence: jdlewis@ualberta.ca
http://dx.doi.org/10.1016/j.celrep.2014.07.050

SUMMARY

Tumor cell extravasation is a key step during cancer metastasis, yet the precise mechanisms that regulate this dynamic process are unclear. We utilized a high-resolution time-lapse intravital imaging approach to visualize the dynamics of cancer cell extravasation in vivo. During intravascular migration, cancer cells form protrusive structures identified as invadopodia by their enrichment of MT1-MMP, cortactin, Tks4, and importantly Tks5, which localizes exclusively to invadopodia. Cancer cells extend invadopodia through the endothelium into the extravascular stroma prior to their extravasation at endothelial junctions. Genetic or pharmacological inhibition of invadopodia initiation (cortactin), maturation (Tks5), or function (Tks4) resulted in an abrogation of cancer cell extravasation and metastatic colony formation in an experimental mouse lung metastasis model. This provides direct evidence of a functional role for invadopodia during cancer cell extravasation and distant metastasis and reveals an opportunity for therapeutic intervention in this clinically important process.

INTRODUCTION

Metastasis is a complex multistep process that represents the most deadly aspect of cancer. Tumor cells that successfully disseminate from the primary tumor and survive in the vascular system eventually extravasate across the endothelium to colonize secondary sites. However, the process of cancer cell extravasation is the least understood step in the metastatic cascade. Immune cell extravasation, or diapedesis, relies on ligand-receptor interactions for adhesion to the endothelium, forming specialized structures called podosomes to facilitate their transit across the endothelial layer (Carman et al., 2007). Morphologically, these podosomes have been described as "invadosome-like protrusions" that are thought to be the normal counterparts of subcellular protrusions that are commonly referred to as invadopodia in cancer cells (Carman and Springer, 2004; Carman et al., 2007; Murphy and Courtneidge, 2011). Podosomes have been observed in vivo during atherogenesis of the intimal layer of mouse aorta (Quintavalle et al., 2010) and in neural crest migration during embryonic development (Murphy et al., 2011), yet a physiological role for invadopodia in cancer has not been established.

Invadopodia are cancer-specific protrusive and adhesive structures that were initially observed in vitro as shallow protrusions on the basolateral side of cultured cancer cells. Extensive efforts to characterize invadopodia and podosomes have revealed that they are composed of structural proteins such as cortactin, N-WASP, Tks4, and Tks5 (Clark et al., 2007; Murphy and Courtneidge, 2011; Oser et al., 2009; Weaver et al., 2002). Of these, Tks5 is exclusively present within podosomes, suggesting that it plays a specific role in invadopodia formation and maturation (Abram et al., 2003; Seals et al., 2005). Invadopodia concentrate proteases such as MT1-MMP, MMP9, and MMP2 for local directed release and/or activity during extracellular matrix breakdown (Clark et al., 2007), and Tks5 is required in both invadopodia and podosomes to degrade matrix in vitro (Caldieri et al., 2009; Furmaniak-Kazmierczak et al., 2007; Magalhaes et al., 2011; Pignatelli et al., 2012; Seals et al., 2005).

The visualization of cancer cell invadopodia in living organisms has been elusive due to the challenges associated with distinguishing them from other invasive structures such as lamellipodia (Gligorijevic et al., 2012). Although established components of invadopodia such as cortactin, MT1-MMP, and Tks4 are also expressed in other protrusive structures including lamellipodia, recent evidence suggests that invadopodia can be specifically inhibited through loss of function of Tks5 (Burger et al., 2014; Diaz et al., 2009; Sharma et al., 2013a). Cytoplasmic extensions formed by tumor cells during intravascular arrest in capillary beds have been observed in zebrafish models (Stoletov et al.,

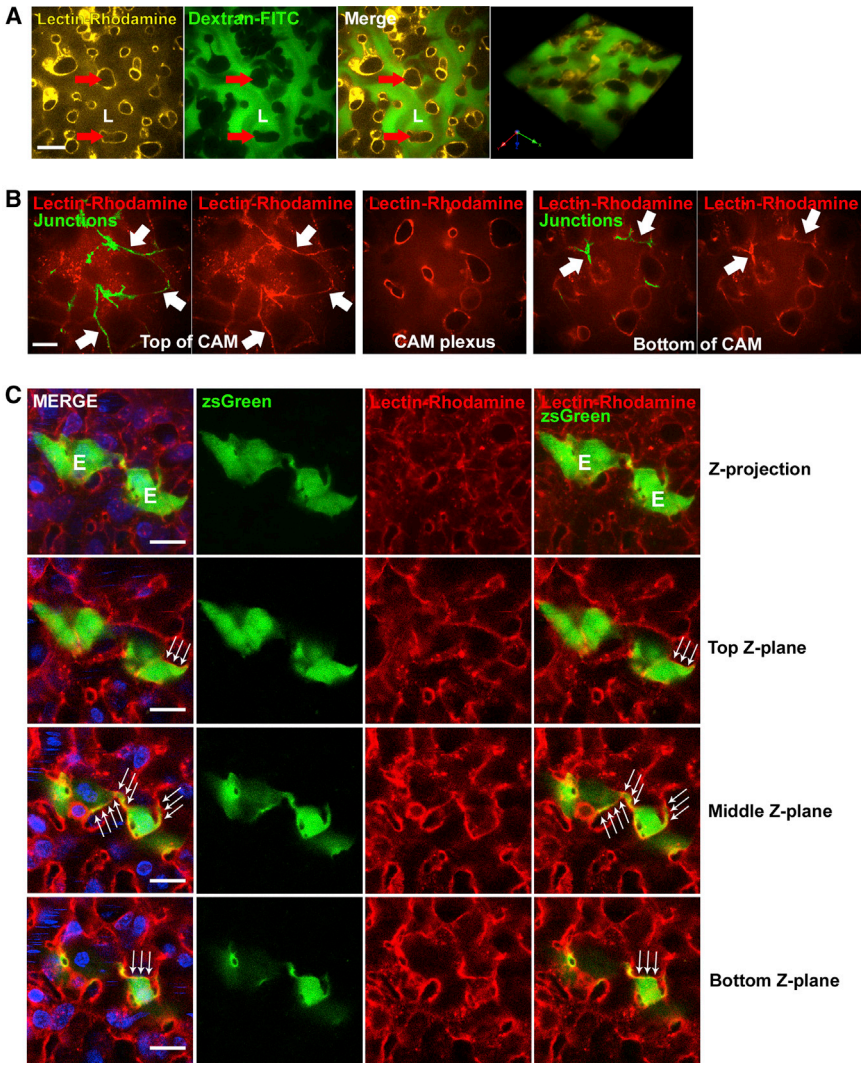

Figure 1. Capillary Plexus, Endothelium, and Endothelial Junction Organization in the Avian Embryo Chorioallantoic Membrane

(A) Lectin-rhodamine labels the luminal surface of endothelial cells and junctions (yellow), whereas dextran-FITC fills the lumen (L) of the capillary bed (green). Scale bar represents 10 μm.

(B) CAM endothelium and endothelial junctions labeled with lectin-rhodamine (red) presented in three different Z planes, top of CAM, CAM plexus, and bottom of CAM. Endothelial junctions are pseudocolored in green. Arrows denote representative endothelial junctions. Scale bar represents 5 μm.

(C) CAM endothelial cells (E) transduced by i.v.-injected lentivirus encoding zsGreen with endothelial junctions labeled by lectin-rhodamine at various Z planes. Endothelial junctions are identified by white arrows that border the two zsGreen-positive endothelial cells. Scale bar represents 10 μm.

2010; Yamauchi et al., 2006), yet a functional link to extravasation has not been established. The visualization and characterization of invadopodia formation in models of breast cancer (Kedrin et al., 2008; Roh-Johnson et al., 2014) have suggested invadopodia as key mediators of intravasation (Eckert et al., 2011; Gligorijevic et al., 2012). Invadopodia have been observed in ex vivo experiments (Schoumacher et al., 2010; Weaver et al., 2013), providing additional support for a role in vivo. However, despite mounting evidence that invadopodia are prevalent in metastatic tumor cells and play a key functional role in the invasion and metastasis of cancer, direct evidence for their contribution in vivo is lacking.

Given the involvement of podosomes in immune cell extravasation and the prevalence of invadopodia in metastatic tumor cells, we sought to investigate the role that invadopodia might play in cancer cell extravasation in vivo. To visualize these dynamic cell interactions in high-resolution detail in real time, we utilized an intravital microscopy platform specifically developed to investigate cancer cell migration in vivo using the ex ovo chicken embryo model (Arpaia et al., 2012; Leong et al., 2010, 2012a, 2012b). In this report, we use real-time 3D time-lapse intravital imaging to visualize the behavior and dynamics of cancer cell extravasation in vivo. We provide direct evidence of the role of invadopodia during cancer cell extravasation. We demonstrate that disruption of invadopodia assembly via interference with structural proteins such as cortactin, Tks4 and Tk5, either by genetic or pharmacological means, results in decreased extravasation efficiency and an abrogation of metastasis.

RESULTS

Intravital Imaging of Human Cancer Cells and Endothelium in Ex Ovo Chicken Embryos

The chorioallantoic membrane (CAM) of the chicken embryo, with its highly organized capillary bed network supported by arteries, veins, and stromal cells, is an ideal model to visualize the behavior of disseminating human tumor cells in vivo (Deryugina and Quigley, 2008; Koop et al., 1996). For these studies, an intravital microscopy platform capable of capturing high-resolution 3D time-lapse imagery of human tumor growth, cell migration, and extravasation using the ex ovo chicken embryo model was utilized (Arpaia et al., 2012; Goulet et al., 2011; Leong et al., 2012a, 2012b; Palmer et al., 2014; Zijlstra et al., 2008). Visualization of the luminal surface of the CAM endothelium is achieved upon intravenous (i.v.) injection of fluorescent *Lens culinaris* agglutinin (Figure 1A, yellow; Movie S1), which interacts specifically with the glyocalyx of avian endothelial cells (Jilani et al., 2003). Blood volume is visualized using i.v. fluorescent dextran (Figure 1A, green; Movie S1). Extravascular regions of the CAM, populated by stromal cells, are readily identified during intravital imaging by their lack of lectin-rhodamine staining (Figure 1A, red arrows). As we have observed previously (Arpaia et al., 2012), a significant accumulation of lectin-rhodamine staining is observed at endothelial

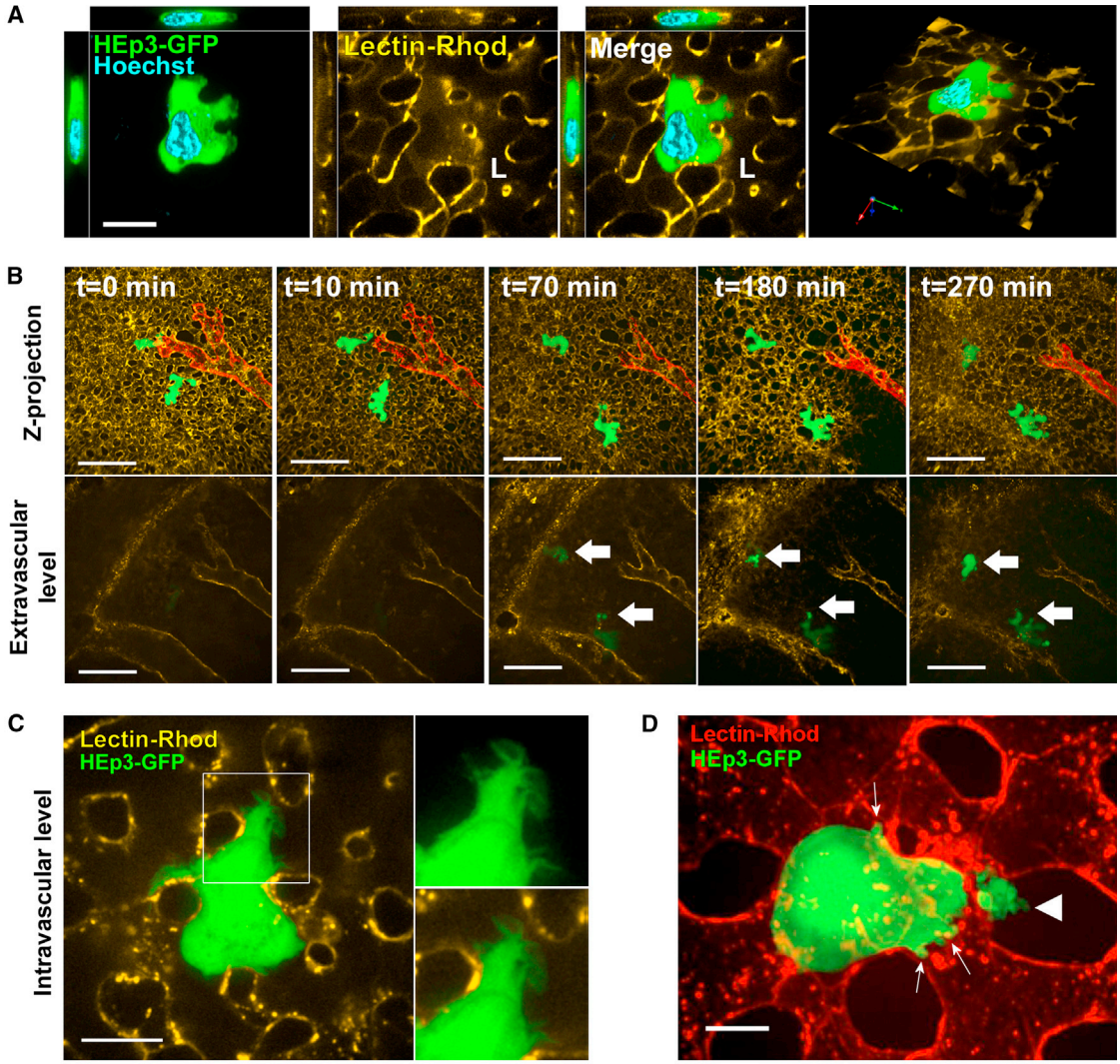

Figure 2. Intravascular Migration of Cancer Cells within the Capillary Bed of the Avian Embryo CAM

(A) HEp3-GFP cell (green) labeled with Hoechst (blue) arrested within the capillary bed. XZ and YZ views of each image are shown for each channel (top and side orthogonal images, respectively; scale bar represents 10 μm.

(B) HEp3-GFP cells undergo intravascular amoeboid migration until they begin projecting protrusions into the extravascular stroma at 70 min postinjection. Scale bars represent 25 μm. The top depicts cells within the intravascular plane, and the bottom represents cells protruding into extravascular stroma. An afferent arteriole that is highlighted in red in the top also represents the large vessel present in the bottom.

(C) HEp3-GFP cell arrested within the CAM forms fan-like projections into the CAM plexus. Scale bar represents 15 μm.

(D) A single intravascular HEp3-GFP cell in the CAM projects protrusions into the intravascular space (small white arrows) and a larger protrusive structure through the endothelium into the adjacent stroma (arrowhead). Scale bar represents 7 μm.

junctions during intravital imaging experiments (Figure 1B; Movie S2, white arrows, junctions pseudocolored green), allowing their precise delineation. To confirm this, the avian endothelium was transduced with cytoplasmic zsGreen in vivo using i.v. lentivirus prior to injection of lectin-rhodamine, which resulted in cytoplasmic GFP expression in roughly 5% of the CAM endothelial cells (Figure 1C). Strong lectin staining corresponded precisely with the endothelial cell-cell junctions when examined using multiple Z views (white arrows, Figure 1C).

Cancer Cells Undergo Intravascular Migration Prior to Extravasation

To define the characteristics of tumor cell arrest and extravasation in this model, time-lapse intravital imaging was performed after the i.v. injection of fluorescent human epidermoid carcinoma (HEp3-GFP) cells into the vitelline vein of ex ovo chicken embryos preinjected with lectin-rhodamine. Circulating tumor cells initially arrest at the distal end of CAM arterioles where they meet the capillary plexus (Figures 2A and 2B, red pseudocolored vessel). Cancer cells conform to the vascular lumen

and adopt an amoeboid morphology, maintaining close contact with the endothelium during intravascular migration (Figure 2B, top), before extravasating into the adjacent stromal layer of the CAM (Figure 2B, bottom; Movie S3). During this process, highly dynamic cytoplasmic protrusions are observed at the leading edge of intravascular HEp3-GFP cells (Figure 2C). Although the majority of these dynamic protrusions are intravascular (Figure 2D, small white arrows), a proportion of these extend through the endothelium into the adjacent stroma (Figure 2D, arrowhead).

Cancer Cells Form Invasive Cytoplasmic Extensions that Breach the Endothelium

Intravital imaging of the early stages of cancer cell extravasation revealed that cancer cells form cytoplasmic protrusions that extend through the endothelium into the extravascular stroma. We observed that cells typically migrate intravascularly along the endothelium for 6–8 hr and then cease migration (Figure 3A, t = 0 hr panel). At this point, protrusions (Figure 3A, t = 0.25 hr panel, yellow arrow; Movie S4) are observed that cross the endothelium into the extravascular stroma. Figure 3B is a full Z projection of an individual cell undergoing extravasation, highlighting the transition of the intravascular (grayscale) and extravascular portions (green) over time. At t = 1.25 hr, the cell has begun extravasation and over the next 3 hr, the extravascular portion (green) grows larger, whereas the intravascular portion (white) gradually shrinks as the cell translocates from the vessel into the stroma (Movie S5). Figure 3C depicts a single cancer cell forming two distinct protrusions (pink and blue arrows) into the extravascular stroma (bottom). However, in all cases observed, cancer cells follow a single protrusion to complete extravasation. These invasive structures were observed in a substantial fraction of a panel of cancer cells, as quantified by intravital imaging (Figure 3D).

The precise route of extravasation was also investigated using high-resolution intravital imaging. When individual planes of 3D image volumes from extravasating HEp3-GFP cells (Figures S1A and S1B) were examined, it was clear that the majority of invasive protrusions project through endothelial junctions that have separated slightly, and that these separations resolve once extravasation is completed (Figure S1D). A panel of cancer cell lines including HT1080 (fibrosarcoma), B16F10 (melanoma), MDA-MB-231LN (breast), and T24 (bladder) were evaluated and found also to extravasate mainly at endothelial junctions (Figure S1C). In some cases, we observed that the cancer cells extensively remodeled the local endothelium, appearing to displace endothelial cells to gain access to the extravascular stroma (Figure S1E). In these cases, the endothelial cells remained viable but did not resolve in the time frame of our experiments. No evidence of interendothelial transit was observed (Carman and Springer, 2008).

Cancer Cells Project Invadopodia through the Endothelium during Cancer Cell Extravasation

We hypothesized that components of invadopodia were present within the cytoplasmic protrusions of extravasating cancer cells observed in vivo. Histology was performed on frozen cross-sectional slices of CAM containing extravasating HT1080 fibrosarcoma cells (Figure 4A). Visualized by fluorescence microscopy, extravasating cells had protrusions (Figure 4A, second panel, white arrows) projecting through the endothelial layer (L, dotted line) and extending into the extravascular stroma (ES). These cell protrusions contain both F-actin (Figure 4A, third panel) and cortactin (Figure 4A, fourth panel), indicating that these protrusive structures might be invadopodia.

To further characterize the identity and dynamics of these protrusions during extravasation, structural components known to be localized or concentrated in invadopodia such as cortactin, Tks4, and Tks5 (Buschman et al., 2009; Oser et al., 2010; Sung et al., 2011; Abram et al., 2003; Seals et al., 2005) were assessed in extravasating cancer cells using intravital imaging. Constructs encoding the fusion proteins cortactin-zsGreen (CTTN-zsG) and Tks4-zsGreen (Tks4-zsG) were stably transfected into three aggressive human cancer cell lines: epidermoid carcinoma HEp3, fibrosarcoma HT1080 (HT1080-tdT), and breast cancer MDA-MB-231LN (231LN-tdT). The localization of each of these was confirmed using fluorescence imaging (Figure S2).

During extravasation of 231LN-tdT cells in vivo, cortactin-zsGreen was abundant in cytoplasmic protrusions extending through the endothelium (Figures 4B and 4C). Although cortactin-zsGreen is also present in foci throughout the cell, the cytoplasmic extension extending into the stromal layer (Figure 4B, bottom; inset) contains organized structures of cortactin-zsGreen that would be expected in invadopodia. Localization of cortactin-zsGreen in HEp3 cells was present as diffuse puncta throughout the cell and within thin invasive structures at the point of extravasation (Figure 4C, arrow). A significant enrichment in cortactin-zsGreen was observed within protrusions that extended through the endothelium (Figure 4C, arrow).

Localization of Tks4-zsG in HEp3, HT1080-tdT and 231LN-tdT cell lines was also evaluated during extravasation using intravital imaging. In intravascular 231LN-tdT breast cancer cells, Tks4-zsGreen was present as diffuse signal throughout the cytoplasm (Figure 4D, upper left; Movie S6). During extravasation, however, Tks4-zsGreen localized to the apical tips of cytoplasmic protrusions extending into the CAM stroma (Figure 4D, upper right; Figure 4D, bottom, white arrow; Movie S6). The localization of Tks5-GFP, in contrast, was concentrated at the base of and throughout the protrusion invading into the extravascular stroma (Figure 4E; Movie S7). A similar concentration at the base of invadopodia was not observed in cells expressing Tks4-zsG. The proteolytic activity of MT1-MMP is a key marker of invadopodia, and it was also observed in protrusions formed by extravasating 231LN-tdT cells (Figure 4F) and HT1080 cancer cells (Figure 4G) expressing MT1-MMP-GFP. The enrichment of cortactin, Tks4, Tks5, and MT1-MMP in these invasive protrusions suggests that they are indeed invadopodia, and our intravital imaging experiments suggest that cancer cells extend invadopodia between endothelial cells and into the extravascular stroma prior to and during extravasation.

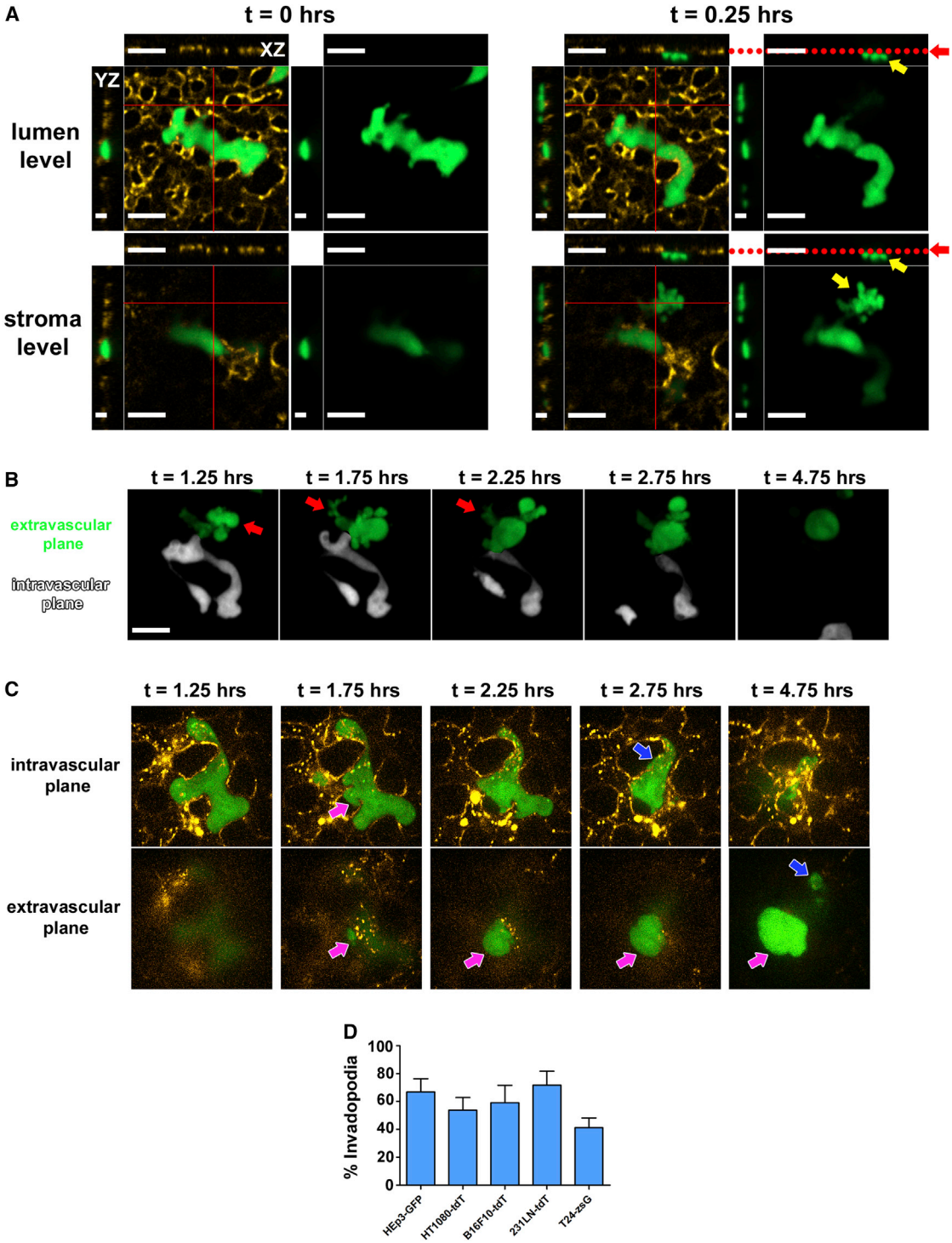

Figure 3. The Formation of Invasive Protrusions Precedes Cancer Cell Extravasation

(A) Formation of invadopodia (yellow arrows) projecting through the endothelial layer (red arrows and red dashed line) into extravascular stroma. Within 15 min (right), a significant protrusion has formed that has projected through the endothelial layer (red arrows and red dashed line). Scale bars in XY and XZ views are 20 μm, whereas scale bar in YZ is 4 μm.

(B) HEp3-GFP cell undergoing extravasation. Green signal represents portion of cell that has extravasated. White signal represents portion of cell that remains within the intravascular space. Invadopodia formation is highly dynamic within the extravascular stroma (red arrows). Scale bar represents 20 μm.

(legend continued on next page)

Tks4, Tks5, and Cortactin Are Required for Invadopodia Formation and Extravasation in the CAM

To understand the impact of invadopodia on extravasation in vivo, we performed loss-of-function experiments targeting Tks4 and Tks5 individually, which has been shown to inhibit invadopodia function in vitro (Buschman et al., 2009; Diaz et al., 2009). We hypothesized that RNAi knockdown of Tks4 or Tks5 would inhibit invadopodia formation in cancer cells, thus abrogating cancer cell extravasation and metastasis. Cancer cell lines with stable small hairpin RNA (shRNA) knockdowns of cortactin (Figure S3A), Tks4, and Tks5 (Figures S3C and S3D) were evaluated for their ability to form invadopodia, to extravasate, and to establish metastatic colonies in vivo. These were compared with cells lacking key cell migration mediator RhoA (Figure S3B). When assessed for their ability to degrade extracellular matrix, loss of cortactin, but not RhoA, reduced the fraction of cells able to degrade gelatin (Figure S3E).

HEp3-GFP cells expressing RhoA or cortactin shRNAs were assessed in extravasation assays with the chick embryo CAM using an intravital imaging approach. Cancer cells arrested in the CAM were visualized (Figures 5D–5F) and classified according to their location as intravascular (Figure 5G), in the process of extravasating (Figure 5H), or extravascular (Figure 5I). The majority of shLuc HEp3-GFP cells (~40%–50%) extravasate within 24 hr (Figure 5I), with very few cells present in the intravascular space (Figure 5G). In contrast, a significantly greater proportion of shCTTN cells remained in the intravascular space at each time point, whereas very few shRhoA cells were present within the intravascular space (Figure 6G). Moreover, very few shRhoA and shCTTN cells successfully extravasated after 24 hr after i.v. injection (Figure 5I). Because the numbers of extravasating cells can be monitored over time in each embryo, the number of cells that have been lost/died can be determined (Figure 5J). Cells expressing shRhoA exhibited the greatest loss between the t = 0 to t = 6 hr time points, indicating that most of these cells likely died in the intravascular space. Cell attrition was much lower in the first 6 hr for shLuc and shCTTN cells, indicating that the significant difference in the numbers of intravascular and extravascular cells after 24 hr was not due to cell death, but due to an inhibition of the shCTTN cells to successfully extravasate.

The impact of cortactin on subsequent metastatic colony formation was then assessed using intravital imaging and an experimental metastasis approach. Two hundred thousand cells/embryo were injected i.v., and after 7 days the number of metastases (Figure 5A), micrometastases (Figure 5B), and single cancer cells (Figure 5C) present throughout the entire CAM organ was enumerated. Embryos injected with shRhoA and shCTTN cells had the fewest metastases, micrometastases, and single cells compared to both parental and shLuc control cells. Taken together, these data indicate that RhoA depletion inhibits metastatic colony formation primarily through cell attrition, whereas the inhibition of invadopodia through the depletion of cortactin inhibits metastasis as a result of decreased cancer cell extravasation.

Although Tks4 is predominantly localized to invadopodia, it has also been observed within lamellipodia, whereas Tks5 has only been observed in invadopodia (Abram et al., 2003; Buschman et al., 2009; Seals et al., 2005). To further establish the requirement of invadopodia for extravasation and metastatic colony formation, 231LN-tdT cell lines with stable shRNA knockdowns for Tks4 and Tks5 (Figures S3C and S3D) were evaluated for their ability to extravasate in the CAM of avian embryos over a 24 hr time period. 231LN-tdT cells lacking RhoA, CTTN, Tks4, or Tks5 had significantly decreased extravasation rates compared to control cells (Figure 5K). Furthermore, these were also observed to have decreased incidence of protrusions formed by cells arrested in the intravascular space (Figure 5L) 3 hr after i.v. injection of cells. Collectively, this provides strong evidence that invadopodia are indeed required for efficient extravasation in the CAM. These in vivo loss-of-function experiments demonstrate a requirement for CTTN, Tks4, and Tks5 in the formation of invadopodia and cancer cell extravasation.

Src Kinase Inhibition Abrogates Invadopodia Formation and Extravasation

Src kinase regulates invadopodia formation via phosphorylation of cortactin to its active state (Evans et al., 2012; Mader et al., 2011; Oser et al., 2009), while also phosphorylating a number of other targets (Ferrando et al., 2012). Treatment of HEp3-GFP cells with the Src kinase inhibitor Saracatinib at 1.0 μM significantly altered in vitro cell morphology from a stellate to cobblestone morphology (Figures 6A and 6B). A marked reduction of cortactin-rich invadopodia and the associated adhesion-type structures that are characteristic of invadopodia was observed (red arrowheads, Figures 6C and 6D). The impact of Src kinase inhibition on the extravasation kinetics of HEp3-GFP cells in the avian embryo CAM was assessed in vivo over a 24 hr time period, comparing Saracatinib at 1.0 μM versus vehicle. No in vivo or in vitro cytotoxic effects were observed when Saracatinib was administered to a final concentration of 1.0 μM (Figure S6). Saracatinib-treated cancer cells at 3–6 hr after i.v. injection exhibited a significant decrease in invadopodia formation compared to vehicle-treated cells (Figure 6E). Over 24 hr, Saracatinib treatment resulted in significantly decreased extravasation rates compared to vehicle control at t = 24 hr (Figures 6G and 6H) accompanied by a retention of Saracatinib-treated cells in the intravascular space at t = 24 hr (Figure 6F). The interpretation of the data is complicated somewhat by the fact that more Saracatinib-treated cells were lost or died in the first 3 hr compared to vehicle-control-treated cells (Figure 6I), resulting in significantly fewer cells successfully extravasating at after 24 hr. Nevertheless, these data suggest that Saracatinib directly impacts cancer cell extravasation, providing a potentially useful therapeutic approach.

(C) A single T24-zsGreen cell undergoing extravasation. The top depicts a single cell forming two different cytoplasmic protrusions (pink and blue arrows) into the extravascular stroma (bottom).

(D) Fraction of cells that form invadopodia as observed using intravital imaging during extravasation in a panel of cancer cell lines (n = 50 cells, three animals). Error bars represent ± SEM.

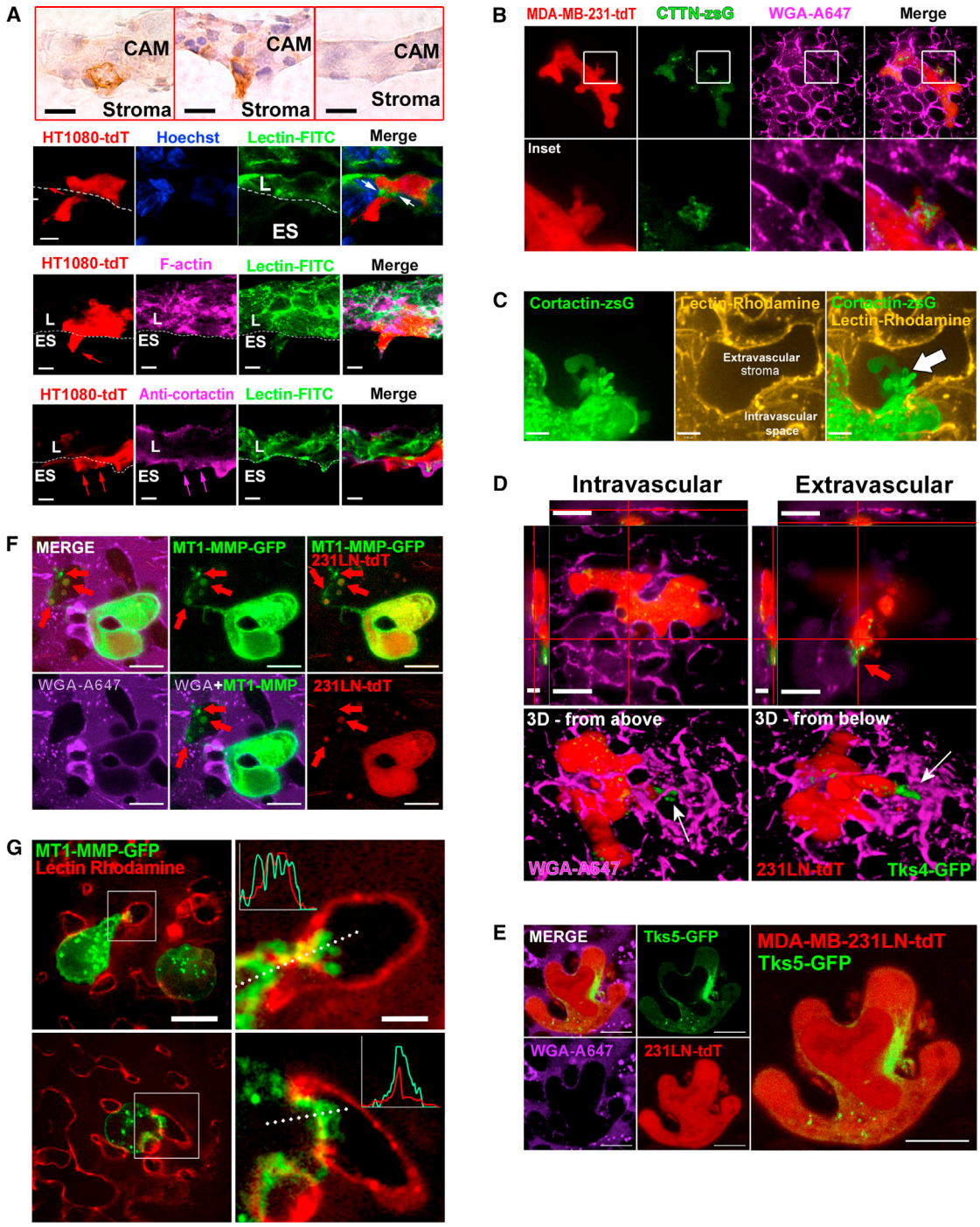

Figure 4. The Formation of Cortactin and Tks4-Positive Invadopodia Precedes Cancer Cell Extravasation in Vivo

(A) Representative HT1080-tdT cells in the CAM that are intravascular (left) or undergoing extravasation (middle). A cross-section of CAM with no cells is also shown (right). The second panel of images shows a single HT1080-tdT cell with a cytoplasmic extension that has projected through the endothelium (labeled with lectin-FITC, green). The dotted line demarcates the extravascular stroma-capillary bed interface. L, capillary bed lumen; ES, extravascular stroma. The third panel shows a single HT1080-tdT cell that has formed a cytoplasmic extension that contains F-actin. The fourth panel shows cytoplasmic extensions formed by a single HT1080-tdT cell that contains cortactin, an invadopodia-specific marker. Scale bars represent 5 μm.

(B) Intravital imaging of a single 231LN-tdT cell prior to extravasation with a CTTN-zsG-rich protrusion (inset).

(C) Intravital imaging of a single CTTN-zsG-expressing HEp3 cell undergoing extravasation into the extravascular stroma. The multilobed structure present within the extravascular stroma has a cortical distribution of CTTN-zsG.

(legend continued on next page)

Inhibition of Tks4 or Tks5 Reduces Metastatic Colony Formation in a Mouse Lung Metastasis Model

Given our observations in the chicken embryo CAM model, we sought to confirm our findings in a mammalian adult cancer model. Clonogenic MDA-MB-231LN-tdT cell lines were generated with stable shRNA knockdowns for Tks4 and Tks5 (Figures S3C and S3D) and evaluated for their ability to extravasate and form metastatic colonies in murine lungs following tail vein injection in nude beige mice. Extravasation efficiency was determined by comparing the number of cells that extravasated at t = 24 hr after i.v. injection to the number of cells that initially arrested in the lung at t = 0 hr after i.v. injection. According to histological sections of injected murine lungs, the majority of cells were intravascular immediately after injection (Figures 7A and 7C, open bars), and all cells that were present in the lungs after 24 hr had successfully extravasated as determined by confocal microscopy (Figures 7B and 7C, filled bars). Knockdown of Tks4 or Tks5 resulted in significant decreases in extravasation compared to shLUC control (Figure 7C). Indeed, the majority of the Tks4 and Tks5 shRNA clones exhibited negligible rates of extravasation, with no extravasated cancer cells visible 24 hr after injection. Metastatic burden was also evaluated at 4 weeks postinjection, where knockdown of Tks4 or Tks5 resulted in a significant decrease in the number of macrometastases (Figure 7D), micrometastases (Figure 7E), and extravascular single cells (Figure 7F). Representative thick-mount sections of lung metastases formed by i.v. injection with the 231LN-tdT shLUC control cells or 231LN-tdT cells expressing the Tks4 or Tks5 shRNA knockdown construct can be found in Figures S4 and S5. Altogether, these data demonstrate in two xenograft models of human cancer metastasis that invadopodia are required for extravasation and metastatic colonization of distant sites.

DISCUSSION

The extravasation of cancer cells at distant sites occurs predominantly within capillary beds (Chambers et al., 2002) and is thought to be a key step in the metastatic cascade, preceding metastatic colony formation. During the past several years, a putative role for invadopodia in cancer cell migration and invasion has been extensively described using in vitro approaches (Artym et al., 2006; Buschman et al., 2009; Diaz et al., 2009; Linder, 2007; Mader et al., 2011; Oser et al., 2009), whereas a lack of direct in vivo evidence for invadopodia has raised questions regarding their physiological relevance in cancer. Using cortactin, MT1-MMP, and Tks4/5 fusion expression constructs and shRNA-mediated knockdown, we have determined that invadopodia are formed early in the extravasation process, manifest as protrusions that project through the endothelial layer, and are required for successful extravasation. Cancer cell extravasation is a highly coordinated and dynamic process that occurs within 24 hr, consistent with observations made many years ago during our initial intravital imaging experiments (Koop et al., 1996). Inhibition of the structural or functional components of invadopodia results in a significant decrease in metastatic colony formation in two experimental models of metastasis. By providing direct evidence of the functional importance of invadopodia in cancer cell extravasation in vivo, these studies demonstrate that invadopodia play a crucial role in the metastatic cascade and represent a potential therapeutic target for antimetastasis strategies.

The assembly of invadopodia is a tightly regulated and sequential process that is characterized by the initial formation of nondegradative invadopodium precursors that are enriched in actin regulators, including cortactin, Arp2/3, and cofilin among others (Clark et al., 2007; Oser et al., 2009). These precursors then mature through a sequence of events that involve stabilization through Tks5 interactions (Blouw et al., 2008), actin polymerization, and the recruitment of matrix proteases such as MT1-MMP, whose localization and stability is further regulated by factors such as Tks4 (Buschman et al., 2009). This results in mature, matrix-degrading invadopodia that coordinate the remodeling of the ECM to promote cell migration and translocation. Based on our observations regarding the ability of invadopodia to project through the endothelial layer in the early steps of cancer cell extravasation, we hypothesized that their inhibition would prevent extravasation and the subsequent formation of metastatic colonies. We investigated the inhibition of distinct steps of invadopodia initiation (cortactin), maturation (Tks5), and function (Tks4) on the extravasation of metastatic cancer cells and compared these to the loss of RhoA, which would be expected to inhibit cell migration in an invadopodia-independent way. Extravasation rates were significantly decreased in the CAM of the avian embryo and mouse lungs when any of these contributors to invadopodia were depleted in cancer cells. The depletion of Tks4 or Tks5 in cancer cells also led to a decrease in micrometastases and single cells compared to control cancer cells, suggesting that the inhibition of invadopodia has additional antimetastatic effects that lead to a further decrease in metastatic efficiency. These observations are consistent with other studies that have established a role for invadopodia in other steps in the metastatic cascade, such as tumor growth and intravasation (Blouw et al., 2008; Gligorijevic et al., 2012; Sharma et al., 2013b), and implicates these structures in a general mechanism for tumor cell motility and translocation.

(D) Single MDA-MB-231-tdT cell expressing Tks4-zsG that is predominantly intravascular but has begun the process of extravasation (left). Tks4-zsG is concentrated at the tip of the cytoplasmic extension, which has extended into the adjacent extravascular stroma (right). Scale bars are XY, 10 μm, and XZ, 3 μm. 3D-rendered images of this cell (red) from above and below the CAM capillary endothelium (magenta) show localization of Tks4-zsG (green) at the apical tip of the invadopodium that is extending into the extravascular stroma.

(E) An individual MDA-MB-231LN-tdT cell expressing Tks5-GFP has compartmentalized the majority of Tks5-GFP signal within the invadopodia, which is invading into the extravascular stroma (S, dotted line). Scale bars represent 10 μm.

(F) An individual MDA-MB-231LN-tdT cell expressing MT1-MMP-GFP has compartmentalized MT1-MMP-GFP in protrusions that are present in the extravascular stroma (red arrows).

(G) HT1080 cells expressing MT1-MMP-GFP (green) project protrusions through the endothelium (red) into the extravascular stroma (black). Invasive protrusions are expanded in the right, and a line scan is provided in order to show that MT1-MMP expression is localized in the protrusion both at the site of contact with the endothelium and beyond the endothelium in the extravascular stroma.

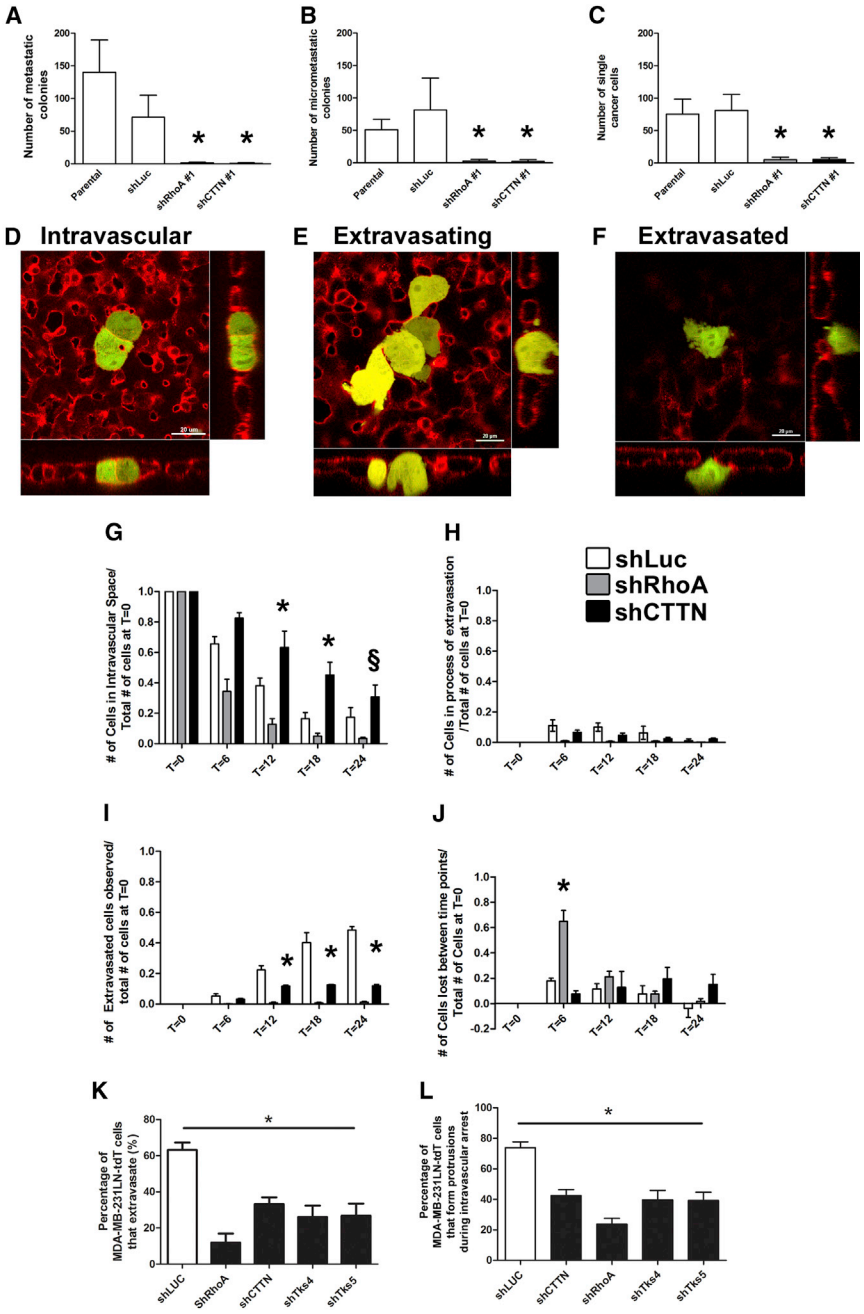

Figure 5. Knockdown of Cortactin and RhoA Results in Decreased Extravasation Efficiency

(A–F) (A) The total number of overt metastases (more than five cells), (B) micrometastases (two to five cells), and (C) single cells found throughout the CAM at 5 days postextravasation. In (A)–(C), *p < 0.05 compared to shLUC. One-way ANOVA with Bonferroni test. n = 8 per group. Representative HEp3-GFP cells imaged within the intravascular space (D), in the process of extravasation (E), and immediately postextravasation (F).

(G–J) White bars denote shLuciferase HEp3-GFP cells. Gray bars denote shRhoA HEp3-GFP cells. Black bars denote shCTTN HEp3-GFP cells. (G) The percentage of cells present within the intravascular space over a 24 hr time frame. *p < 0.05 compared to shLUC and shRhoA. §p < 0.01 compared to shRhoA. (H) The percentage of cells observed to be actively in the process of extravasation. (I) The percentage of cells present within the extravascular stroma. *p < 0.01 compared to shLUC and shRhoA. (J) The percentage of cells lost/died at each 6 hr time frame throughout the 24 hr time frame of analysis. *p < 0.001 compared to shLUC and shCTTN. In (G)–(J), experiments consisted of n = 3, >400 cells per animal. Two-way ANOVA with Bonferroni test was used for (G)–(J).

(K) Extravasation efficiency assay of MDA-MB-231LN-tdT cells with shLUC (white bar), shRhoA, shCTTN, and shTks4/5 (black bars) over a 24 hr time course. * p < 0.01 compared to shLUC, n > 100 cells counted for each animal, n > 5 for each group.

(L) Quantitation of protrusions formed by intravascular arrested cells in K) at 3 hr after i.v. injection of cells. *p < 0.01 compared to shLUC, n > 50 cells counted for each animal, n > 5 for each group. Error bars represent ± SEM.

We have established that the inhibition of extravasation by targeting invadopodia is a viable antimetastasis approach. Nonetheless, a clinical window of opportunity for antimetastatic therapies may not exist for all cancer patients, especially considering the primary tumor's ability to disseminate cancer cells into the circulation at early stages of progression. However, there may be therapeutic opportunities at distinct stages of cancer development and treatment that are worthy of additional study. A substantial body of clinical evidence suggests cancers with an extended natural history, such as prostate cancer, acquire metastatic potential during the course of progression. Thus, some benefit from antimetastasis agents might be realized for patients that are identified at increased risk of metastasis (Palmer et al., 2014). Additionally, a therapeutic approach targeting extravasation directly could be evaluated for cancers that require neoadjuvant treatment to reduce the size of the tumor for subsequent surgical resection, offering the opportunity to also interfere with extravasation of cancer cells shed during treatment. Finally, based on growing evidence that cancer cells are shed into the circulation subsequent to core-needle biopsy (Hansen et al., 2004) or surgery (Juratli et al., 2014), it would be worth exploring whether an antiextravasation approach could help to mitigate any potential risk from these procedures.

Our understanding of cancer cell extravasation has been informed to a significant extent by well-characterized mechanisms of immune cell transendothelial migration or diapedesis. This study both clarifies and substantiates our concepts of cancer cell extravasation through the dynamic visualization of individual cancer cells at high resolution. Although the processes

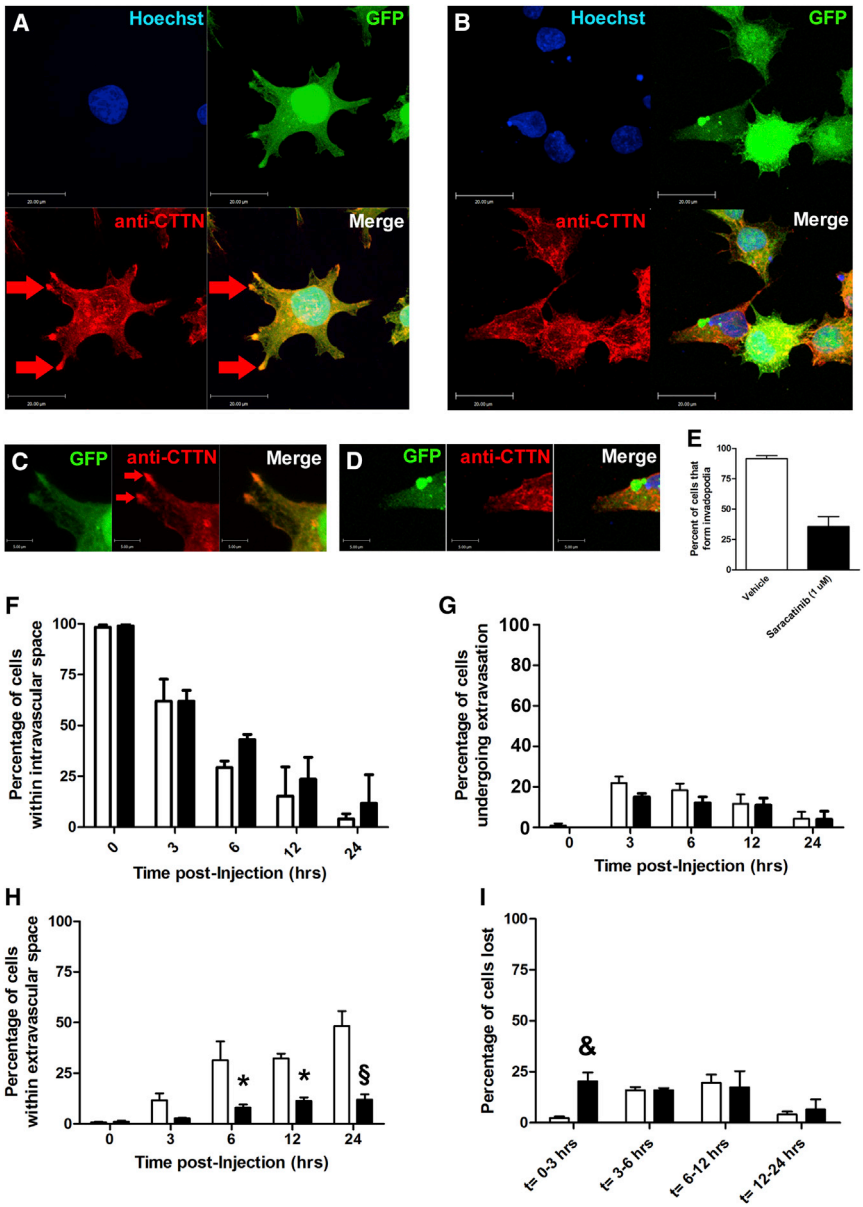

Figure 6. Saracatinib, a Src Kinase Inhibitor, Decreases Cancer Cell Extravasation In Vivo

(A) Representative confocal laser scanning micrograph of HEp3-GFP cells immunostained with antibodies specific for human cortactin (CTTN).

(B) Treatment with Saracatinib (1 μM final) shows a lack of cortactin-rich membrane ruffles and adhesion-type structures.

(C) High magnification of cortactin-rich membrane adhesion-type structures formed by HEp3-GFP cells.

(D) Saracatinib treatment results in the loss of adhesion-type structures formed by HEp3-GFP cells.

(E) Saracatinib inhibits invadopodia formation in vivo over a 3 hr time frame prior to extravasation ($n > 200$ cells per group).

(F–I) Extravasation efficiency assay using HEp3-GFP cells treated with vehicle (white bars) and 1 μM Saracatinib (black bars). The percentage of cells present within the intravascular space (F), in the process of extravasation (G), within the extravascular stroma (H), and the percentage of cells lost/died between each time frame (I). *$p < 0.05$ compared to vehicle treatment. §$p < 0.001$ compared to vehicle treatment. One-way ANOVA with Bonferroni test. &$p < 0.05$ compared to vehicle treatment at t = 0, Student's t test.

Error bars represent ± SEM.

of cancer cell extravasation and leukocyte diapedesis share several common features (Carman and Springer, 2008), we did not see any evidence in our intravital imaging experiments that cancer cells undergo transcellular migration, or migration through pores created in endothelial cells, as seen with leukocytes. Our examination of thousands of cells from a panel of cancer cell lines undergoing extravasation demonstrated clearly that cancer cells in this model system utilize a paracellular route of transendothelial migration into the extravascular stroma. The simplest explanation for this is due to the fact that cancer cells are typically much larger in volume than leukocytes or endothelial cells. We did observe that a minority of extravasating cells gained access to the extravascular stroma by a more dramatic displacement of endothelial cells. This did not appear to impact the viability of the endothelial cells and is consistent with previous observations in an in vivo model (Stoletov et al., 2010) that suggests that tumor cells can play an active role in remodeling the local endothelium. This is particularly interesting in light of a recent report that links invadopodia biogenesis with the secretion of exosomes (Hoshino et al., 2013). In our intravital imaging experiments, invadopodia were quite dynamic in morphology as they extended into the extravascular stroma and were sporadically associated with the transient release of microparticles. The idea that invadopodia utilize a tightly regulated microvesicle release mechanism to influence the local microenvironment is a compelling one and warrants further investigation. Overall, we have established a powerful model to visualize and dissect the key functional and structural components of invadopodia and provide unequivocal evidence for a role for invadopodia during cancer cell extravasation.

EXPERIMENTAL PROCEDURES

Cells, Antibodies, and Reagents

The human epidermoid carcinoma cell line HEp3, human breast cancer cell lines MDA-MB-435, MDA-MB-468, MDA-MB-231-luc-D3H2LN (termed MDA-MB-231LN or 231LN), fibrosarcoma cell line HT1080, and human bladder cancer cell line T24 were all maintained as described previously (Leong et al., 2012a; Vantyghem et al., 2005; Zijlstra et al., 2008). Lectin-Rhodamine/Fluorescein

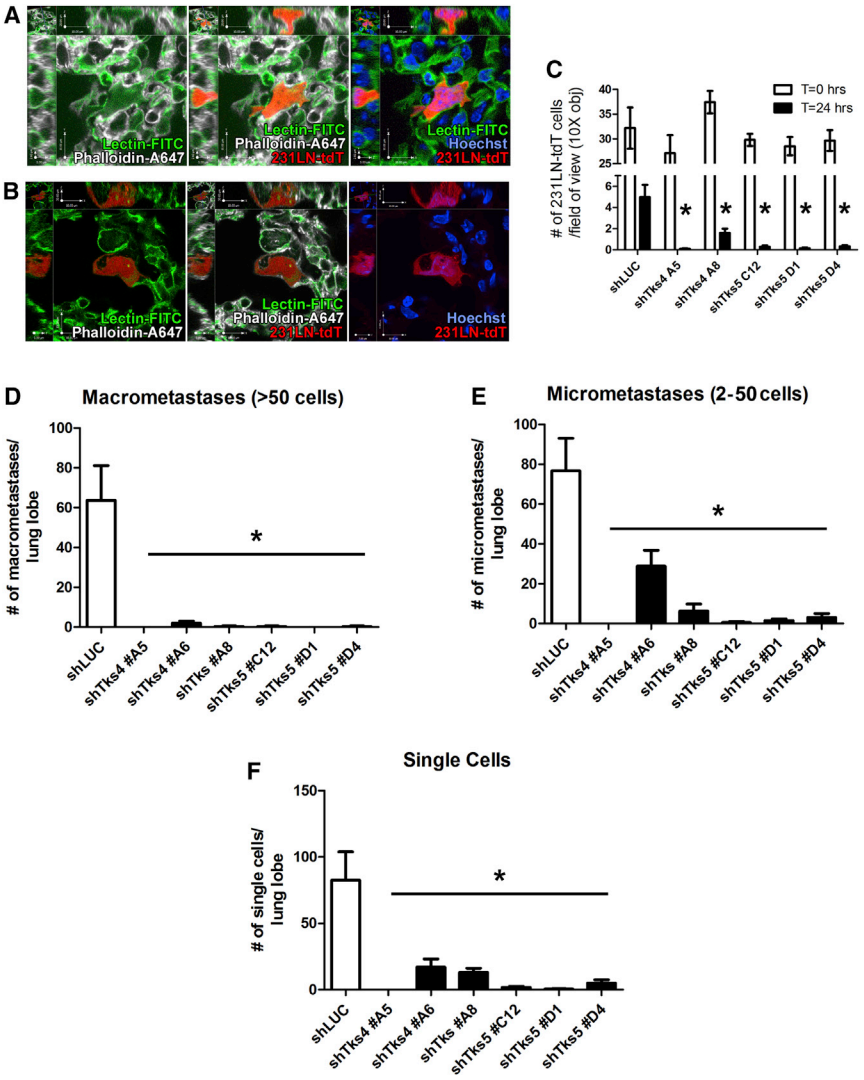

Figure 7. Invadopodia-Specific Tks4 and Tk5 Are Required for Extravasation and the Formation of Metastases

(A) Representative MDA-MB-231LN-tdT cell arrested within a microvessel as identified by Lectin-FITC and Phalloidin-A647 reveals stroma.

(B) Extravasated cell present within lung stroma.

(C) Extravasation efficiency of MDA-MB-231LN-tdT cells with shLUC, shTks4, or shTks5 knockdown constructs in the mouse lung. White bars represent 231LN cells observed in a random field in mouse lung sections at t = 0, and the black bars represent the number of 231LN cells observed in mouse lung sections at t = 24 hr. *p < 0.05 compared to shLUC t = 24 hr, two-way ANOVA, Bonferroni test. n = 5 mice per cell line at each time point.

(D–F) (D) The number of macrometastases (more than 50 cells observed in single colony), micrometastases (E), and single cells (F) present in mouse lung sections from mice i.v. injected with 231LN cells with shLUC, shTks4, and shTks5 knockdown constructs. *p < 0.05 compared to shLUC, one-way ANOVA. For (D)–(F), n = 8 mice were used for each cell type/shRNA clone.

Error bars represent ± SEM.

conjugates (*Lens culinaris* Agglutinin, Vector Laboratories) and Wheat Germ Agglutinin-Alexa 647 (Invitrogen) were diluted 20 times with 1 × PBS (pH 7.4). Vectors pzsGreen-C1 (Clontech) and pTdTomato (kindly provided by Dr. Roger Tsien, UCSD) were stably transfected into cancer cell lines with Superfect (QIAGEN). Cortactin and luciferase shRNA constructs were kindly provided by Dr. Jason Moffat and the Ontario Institute for Cancer Research (OICR) Genomics Facility. The Src kinase inhibitor Saracatinib (AZD0530) was provided by AstraZeneca and diluted into 10 mM stocks with DMSO and then diluted with PBS for injections. Antibodies specific for cortactin, Tks4, and Tks5 were from Cell Signaling Technology and phalloidin-A647 was from Invitrogen. The cortactin cDNA was acquired from the OICR Genomics Facility. Cortactin and Tks4 coding regions were PCR amplified without the stop codon and inserted within the BamH1-Age1 site of the pzsGreen-C1 vector (Clontech). Primers were designed such that an Ala-Ala-Leu-Pro-Val-Ala-Thr (A-A-L-P-V-A-T) linker was engineered between the target and the zsGreen coding sequence. The ALPVAT linker is endogenous to the original surrogate vector.

The Ex Ovo Chick Embryo Model for Visualization of Cancer Cell Extravasation and Metastasis

To label the luminal surface and endothelial junctions within the CAM, 50 μl of Lectin-Rhodamine/Fluorescein or Wheat Germ Agglutinin-A647 was intravenously injected using a disposable micropipette syringe as described previously (Leong et al., 2012b). After 10 min of lectin microinjection, cancer cells were injected and imaged as described previously (Leong et al., 2012a). The experimental metastasis assays were performed as described previously (Zijlstra et al., 2008). Velocity software (Perkin-Elmer) was used for the acquisition of 4D data sets and used in combination with ImageJ (NIH) for image analysis. To label the cytoplasm of individual endothelial cells within the CAM, 75 μl of zsGreen-encoding lentivirus was injected into D9 avian embryos and then subsequently injected at D14 with 50 μl of Lectin-Rhodamine to label endothelial junctions. ZsGreen-lentivirus was generously provided by Dr. Jason Moffat.

Histology of Cancer Cell Extravasation In Vivo

Histology of cancer cells undergoing extravasation was performed by intravenous injection of lectin-fluorescein and 5 × 10^6 HT1080-tdT cells into the CAM, and tissue was removed and fixed in formalin + 25% sucrose overnight. CAM tissue was embedded in OCT for frozen sectioning at 5 μm thickness. For immunohistochemistry of CAM cross-sections with HT0180-tdT cells undergoing extravasation, anti-CD44 monoclonal antibody (mAb) (clone 29-7) was used for primary antibody staining followed by goat anti-mouse immunoglobulin (Ig) G-HRP secondary antibody staining. The anticortactin mAb and its secondary antibody stain, goat anti-mouse IgG-Alexa 594, and phalloidin-Alexa 647 were used to stain for invadopodia in cancer cells.

Quantitative RT-PCR and Western Immunoblot Analysis

Total RNA was extracted from trypsinized cells with Trizol (Invitrogen). RNA (1 μg) was reverse transcribed into cDNA by random priming using the One-Step RT-PCR Kit (QIAGEN). Quantification of cDNA was done using SYBR Green Supermix for real-time qPCR (Bio-Rad) with oligonucleotide sequences that specifically recognize GAPDH, RhoA, cortactin, Tks4, and Tks5. GAPDH was used as a control for total cDNA. Samples for western immunoblot

analysis were prepared by lysing 2 × 10^6 cells of interest with 200 μl of RIPA buffer (0.05% protease inhibitor cocktail, Roche Scientific) and incubating on ice for 15 min, centrifugation of samples at 4°C at 8,000 × *g* for 10 min, reserving the protein lysate supernatant for SDS-PAGE. After protein quantitation by Bio-Rad protein assay reagent using BSA as a standard, 20 μg of protein was loaded and submitted to SDS-PAGE electrophoresis on 8% SDS-PAGE gels and transferred onto a nitrocellulose membrane (Amersham). Membranes were blocked in 5% skim milk in TBS-T and incubated with the indicated primary antibody overnight at 4°C. After multiple PBS washes, membranes were then incubated with horseradish peroxidase-conjugated secondary antibodies for 1 hr and then were detected using ECL plus western blotting detection system (Amersham).

Avian Embryo CAM Extravasation Efficiency Assay

HEp3-GFP cells with cortactin, RhoA, or Luciferase shRNA knockdowns were injected intravenously into the CAM (n > 5 per group) and the proportion of cells in the intravascular space, in the process of extravasation and having extravasated were enumerated in a marked 1 cm × 1 cm area over a 24 hr period. At t = 0 postinjection, all cells were assumed to be intravascular, and, at t = 6 and t = 18, 75 μl of lectin-rhodamine (Vector Labs) was injected intravenously prior to enumeration. Using spinning disk confocal microscopy, individual cells were enumerated, and its phase (intravascular, process of, extravascular) was determined at t = 6, 12, 18, and 24 hr postinjection. At least 100 cells per region of interest were examined for each animal. Hep3-GFP cells were also pretreated with 1 μM of Saracatinib overnight prior to injection into the CAM (n > 5 per group), and the proportion of cells in each plane (intravascular, process of, extravascular) was evaluated as described above with the cells submitted to shRNA knockdown. For metastatic colony formation endpoint assays, cells were also injected intravenously into CAMs (n ≥ 8 per group) and the evaluated at t = 7 days postinjection. The number of macrometastatic colonies (>20 cells), micrometastatic colonies (<20 and greater than two cells), and single cells were enumerated across the entire CAM of the avian embryo.

Mouse Experimental Metastasis Lung Assay and Extravasation Efficiency Assay

MDA-MB-231LN cells with Tks4/5 or Luciferase shRNA knockdowns were injected intravenously in tail veins of 8-week-old female nude beige mice. To evaluate extravasation efficiency, 2.5 × 10^5 of each cell line was injected (n = 5 each time point/group), and lungs were harvested t = 24 hr postinjection. One hundred microliters of *Griffonia simplicifolia* agglutinin-1-fluorescein isothiocyanate (FITC) (GSA-1-FITC, 10× dilution in PBS, Vector Labs) was injected prior to lung harvesting. To evaluate metastatic colony formation, 2.5 × 10^5 of each cell line was injected (n = 8 per group), and lungs were harvested 4 weeks postinjection. All mouse lungs were fixed in formaline + 25% sucrose overnight. Frozen sections of all harvested lungs consisted of 5-μm-thick sections taken every tenth section. Phalloidin-Alexa 647 was also used alongside the GSA-1-FITC signal to distinguish extravasated cells from intravascular cells within the lung tissue. For extravasation efficiency analysis, slides were also stained with Hoechst 33258 (2500X dilution) for 10 min prior to mounting with ProLong Gold (Invitrogen). In all other cases, ProLong Gold + DAPI (Invitrogen) was used to mount all tissues. All animals (nude beige mice, avian embryos) were housed, maintained, and treated by procedures approved by University of Western Ontario and London Health Sciences Centre Institutional Animal Care and Use Committees (IACUC).

SUPPLEMENTAL INFORMATION

Supplemental Information includes six figures and seven movies and can be found with this article online at http://dx.doi.org/10.1016/j.celrep.2014.07.050.

ACKNOWLEDGMENTS

This study was supported by Canadian Cancer Society Research Institute Grant #700537 to J.D.L. and an NSERC Discovery Grant to J.D.L. and E.A.T. J.D.L. holds the Frank and Carla Sojonky Chair in Prostate Cancer Research supported by the Alberta Cancer Foundation. H.S.L. was funded by a Canadian Breast Cancer Foundation Postdoctoral Fellowship grant and the Movember Prostate Cancer Canada Rising Stars Grant. A.F.C. is Canada Research Chair in Oncology, supported by the Canada Research Chairs Program.

Received: December 10, 2013
Revised: June 11, 2014
Accepted: July 25, 2014
Published: August 28, 2014

REFERENCES

Abram, C.L., Seals, D.F., Pass, I., Salinsky, D., Maurer, L., Roth, T.M., and Courtneidge, S.A. (2003). The adaptor protein fish associates with members of the ADAMs family and localizes to podosomes of Src-transformed cells. J. Biol. Chem. *278*, 16844–16851.

Arpaia, E., Blaser, H., Quintela-Fandino, M., Duncan, G., Leong, H.S., Ablack, A., Nambiar, S.C., Lind, E.F., Silvester, J., Fleming, C.K., et al. (2012). The interaction between caveolin-1 and Rho-GTPases promotes metastasis by controlling the expression of alpha5-integrin and the activation of Src, Ras and Erk. Oncogene *31*, 884–896.

Artym, V.V., Zhang, Y., Seillier-Moiseiwitsch, F., Yamada, K.M., and Mueller, S.C. (2006). Dynamic interactions of cortactin and membrane type 1 matrix metalloproteinase at invadopodia: defining the stages of invadopodia formation and function. Cancer Res. *66*, 3034–3043.

Blouw, B., Seals, D.F., Pass, I., Diaz, B., and Courtneidge, S.A. (2008). A role for the podosome/invadopodia scaffold protein Tks5 in tumor growth in vivo. Eur. J. Cell Biol. *87*, 555–567.

Burger, K.L., Learman, B.S., Boucherle, A.K., Sirintrapun, S.J., Isom, S., Díaz, B., Courtneidge, S.A., and Seals, D.F. (2014). Src-dependent Tks5 phosphorylation regulates invadopodia-associated invasion in prostate cancer cells. Prostate *74*, 134–148.

Buschman, M.D., Bromann, P.A., Cejudo-Martin, P., Wen, F., Pass, I., and Courtneidge, S.A. (2009). The novel adaptor protein Tks4 (SH3PXD2B) is required for functional podosome formation. Mol. Biol. Cell *20*, 1302–1311.

Caldieri, G., Giacchetti, G., Beznoussenko, G., Attanasio, F., Ayala, I., and Buccione, R. (2009). Invadopodia biogenesis is regulated by caveolin-mediated modulation of membrane cholesterol levels. J. Cell. Mol. Med. *13* (8B), 1728–1740.

Carman, C.V., and Springer, T.A. (2004). A transmigratory cup in leukocyte diapedesis both through individual vascular endothelial cells and between them. J. Cell Biol. *167*, 377–388.

Carman, C.V., and Springer, T.A. (2008). Trans-cellular migration: cell-cell contacts get intimate. Curr. Opin. Cell Biol. *20*, 533–540.

Carman, C.V., Sage, P.T., Sciuto, T.E., de la Fuente, M.A., Geha, R.S., Ochs, H.D., Dvorak, H.F., Dvorak, A.M., and Springer, T.A. (2007). Transcellular diapedesis is initiated by invasive podosomes. Immunity *26*, 784–797.

Chambers, A.F., Groom, A.C., and MacDonald, I.C. (2002). Dissemination and growth of cancer cells in metastatic sites. Nat. Rev. Cancer *2*, 563–572.

Clark, E.S., Whigham, A.S., Yarbrough, W.G., and Weaver, A.M. (2007). Cortactin is an essential regulator of matrix metalloproteinase secretion and extracellular matrix degradation in invadopodia. Cancer Res. *67*, 4227–4235.

Deryugina, E.I., and Quigley, J.P. (2008). Chick embryo chorioallantoic membrane model systems to study and visualize human tumor cell metastasis. Histochem. Cell Biol. *130*, 1119–1130.

Diaz, B., Shani, G., Pass, I., Anderson, D., Quintavalle, M., and Courtneidge, S.A. (2009). Tks5-dependent, nox-mediated generation of reactive oxygen species is necessary for invadopodia formation. Sci. Signal. *2*, ra53.

Eckert, M.A., Lwin, T.M., Chang, A.T., Kim, J., Danis, E., Ohno-Machado, L., and Yang, J. (2011). Twist1-induced invadopodia formation promotes tumor metastasis. Cancer Cell *19*, 372–386.

Evans, J.V., Ammer, A.G., Jett, J.E., Bolcato, C.A., Breaux, J.C., Martin, K.H., Culp, M.V., Gannett, P.M., and Weed, S.A. (2012). Src binds cortactin through an SH2 domain cystine-mediated linkage. J. Cell Sci. *125*, 6185–6197.

Ferrando, I.M., Chaerkady, R., Zhong, J., Molina, H., Jacob, H.K.C., Herbst-Robinson, K., Dancy, B.M., Katju, V., Bose, R., Zhang, J., et al. (2012). Identification of targets of c-Src tyrosine kinase by chemical complementation and phosphoproteomics. Mol. Cell. Proteomics *11*, 355–369.

Furmaniak-Kazmierczak, E., Crawley, S.W., Carter, R.L., Maurice, D.H., and Côté, G.P. (2007). Formation of extracellular matrix-digesting invadopodia by primary aortic smooth muscle cells. Circ. Res. *100*, 1328–1336.

Gligorijevic, B., Wyckoff, J., Yamaguchi, H., Wang, Y., Roussos, E.T., and Condeelis, J. (2012). N-WASP-mediated invadopodium formation is involved in intravasation and lung metastasis of mammary tumors. J. Cell Sci. *125*, 724–734.

Goulet, B., Kennette, W., Ablack, A., Postenka, C.O., Hague, M.N., Mymryk, J.S., Tuck, A.B., Giguère, V., Chambers, A.F., and Lewis, J.D. (2011). Nuclear localization of maspin is essential for its inhibition of tumor growth and metastasis. Lab. Invest. *91*, 1181–1187.

Hansen, N.M., Ye, X., Grube, B.J., and Giuliano, A.E. (2004). Manipulation of the primary breast tumor and the incidence of sentinel node metastases from invasive breast cancer. Arch. Surg. *139*, 634–639, discussion 639–640.

Hoshino, D., Kirkbride, K.C., Costello, K., Clark, E.S., Sinha, S., Grega-Larson, N., Tyska, M.J., and Weaver, A.M. (2013). Exosome secretion is enhanced by invadopodia and drives invasive behavior. Cell Rep *5*, 1159–1168.

Jilani, S.M., Murphy, T.J., Thai, S.N.M., Eichmann, A., Alva, J.A., and Iruela-Arispe, M.L. (2003). Selective binding of lectins to embryonic chicken vasculature. J. Histochem. Cytochem. *51*, 597–604.

Juratli, M.A., Sarimollaoglu, M., Siegel, E.R., Nedosekin, D.A., Galanzha, E.I., Suen, J.Y., and Zharov, V.P. (2014). Real-time monitoring of circulating tumor cell release during tumor manipulation using in vivo photoacoustic and fluorescent flow cytometry. Head Neck *36*, 1207–1215.

Kedrin, D., Gligorijevic, B., Wyckoff, J., Verkhusha, V.V., Condeelis, J., Segall, J.E., and van Rheenen, J. (2008). Intravital imaging of metastatic behavior through a mammary imaging window. Nat. Methods *5*, 1019–1021.

Koop, S., Schmidt, E.E., MacDonald, I.C., Morris, V.L., Khokha, R., Grattan, M., Leone, J., Chambers, A.F., and Groom, A.C. (1996). Independence of metastatic ability and extravasation: metastatic ras-transformed and control fibroblasts extravasate equally well. Proc. Natl. Acad. Sci. USA *93*, 11080–11084.

Leong, H.S., Steinmetz, N.F., Ablack, A., Destito, G., Zijlstra, A., Stuhlmann, H., Manchester, M., and Lewis, J.D. (2010). Intravital imaging of embryonic and tumor neovasculature using viral nanoparticles. Nat. Protoc. *5*, 1406–1417.

Leong, H.S., Lizardo, M.M., Ablack, A., McPherson, V.A., Wandless, T.J., Chambers, A.F., and Lewis, J.D. (2012a). Imaging the impact of chemically inducible proteins on cellular dynamics in vivo. PLoS ONE *7*, e30177.

Leong, H.S., Chambers, A.F., and Lewis, J.D. (2012b). Assessing cancer cell migration and metastatic growth in vivo in the chick embryo using fluorescence intravital imaging. Methods Mol. Biol. *872*, 1–14.

Linder, S. (2007). The matrix corroded: podosomes and invadopodia in extracellular matrix degradation. Trends Cell Biol. *17*, 107–117.

Mader, C.C., Oser, M., Magalhaes, M.A.O., Bravo-Cordero, J.J., Condeelis, J., Koleske, A.J., and Gil-Henn, H. (2011). An EGFR-Src-Arg-cortactin pathway mediates functional maturation of invadopodia and breast cancer cell invasion. Cancer Res. *71*, 1730–1741.

Magalhaes, M.A.O., Larson, D.R., Mader, C.C., Bravo-Cordero, J.J., Gil-Henn, H., Oser, M., Chen, X., Koleske, A.J., and Condeelis, J. (2011). Cortactin phosphorylation regulates cell invasion through a pH-dependent pathway. J. Cell Biol. *195*, 903–920.

Murphy, D.A., and Courtneidge, S.A. (2011). The 'ins' and 'outs' of podosomes and invadopodia: characteristics, formation and function. Nat. Rev. Mol. Cell Biol. *12*, 413–426.

Murphy, D.A., Diaz, B., Bromann, P.A., Tsai, J.H., Kawakami, Y., Maurer, J., Stewart, R.A., Izpisúa-Belmonte, J.C., and Courtneidge, S.A. (2011). A Src-Tks5 pathway is required for neural crest cell migration during embryonic development. PLoS ONE *6*, e22499.

Oser, M., Yamaguchi, H., Mader, C.C., Bravo-Cordero, J.J., Arias, M., Chen, X., Desmarais, V., van Rheenen, J., Koleske, A.J., and Condeelis, J. (2009). Cortactin regulates cofilin and N-WASp activities to control the stages of invadopodium assembly and maturation. J. Cell Biol. *186*, 571–587.

Oser, M., Mader, C.C., Gil-Henn, H., Magalhaes, M., Bravo-Cordero, J.J., Koleske, A.J., and Condeelis, J. (2010). Specific tyrosine phosphorylation sites on cortactin regulate Nck1-dependent actin polymerization in invadopodia. J. Cell Sci. *123*, 3662–3673.

Palmer, T.D., Martínez, C.H., Vasquez, C., Hebron, K.E., Jones-Paris, C., Arnold, S.A., Chan, S.M., Chalasani, V., Gomez-Lemus, J.A., Williams, A.K., et al. (2014). Integrin-free tetraspanin CD151 can inhibit tumor cell motility upon clustering and is a clinical indicator of prostate cancer progression. Cancer Res. *74*, 173–187.

Pignatelli, J., Tumbarello, D.A., Schmidt, R.P., and Turner, C.E. (2012). Hic-5 promotes invadopodia formation and invasion during TGF-β-induced epithelial-mesenchymal transition. J. Cell Biol. *197*, 421–437.

Quintavalle, M., Elia, L., Condorelli, G., and Courtneidge, S.A. (2010). MicroRNA control of podosome formation in vascular smooth muscle cells in vivo and in vitro. J. Cell Biol. *189*, 13–22.

Roh-Johnson, M., Bravo-Cordero, J.J., Patsialou, A., Sharma, V.P., Guo, P., Liu, H., Hodgson, L., and Condeelis, J. (2014). Macrophage contact induces RhoA GTPase signaling to trigger tumor cell intravasation. Oncogene *33*, 4203–4212.

Schoumacher, M., Goldman, R.D., Louvard, D., and Vignjevic, D.M. (2010). Actin, microtubules, and vimentin intermediate filaments cooperate for elongation of invadopodia. J. Cell Biol. *189*, 541–556.

Seals, D.F., Azucena, E.F., Jr., Pass, I., Tesfay, L., Gordon, R., Woodrow, M., Resau, J.H., and Courtneidge, S.A. (2005). The adaptor protein Tks5/Fish is required for podosome formation and function, and for the protease-driven invasion of cancer cells. Cancer Cell *7*, 155–165.

Sharma, V.P., Eddy, R., Entenberg, D., Kai, M., Gertler, F.B., and Condeelis, J. (2013a). Tks5 and SHIP2 regulate invadopodium maturation, but not initiation, in breast carcinoma cells. Curr. Biol. *23*, 2079–2089.

Sharma, V.P., Entenberg, D., and Condeelis, J. (2013b). High-resolution live-cell imaging and time-lapse microscopy of invadopodium dynamics and tracking analysis. Methods Mol. Biol. *1046*, 343–357.

Stoletov, K., Kato, H., Zardouzian, E., Kelber, J., Yang, J., Shattil, S., and Klemke, R. (2010). Visualizing extravasation dynamics of metastatic tumor cells. J. Cell Sci. *123*, 2332–2341.

Sung, B.H., Zhu, X., Kaverina, I., and Weaver, A.M. (2011). Cortactin controls cell motility and lamellipodial dynamics by regulating ECM secretion. Curr. Biol. *21*, 1460–1469.

Vantyghem, S.A., Allan, A.L., Postenka, C.O., Al-Katib, W., Keeney, M., Tuck, A.B., and Chambers, A.F. (2005). A new model for lymphatic metastasis: development of a variant of the MDA-MB-468 human breast cancer cell line that aggressively metastasizes to lymph nodes. Clin. Exp. Metastasis *22*, 351–361.

Weaver, A.M., Heuser, J.E., Karginov, A.V., Lee, W.L., Parsons, J.T., and Cooper, J.A. (2002). Interaction of cortactin and N-WASp with Arp2/3 complex. Curr. Biol. *12*, 1270–1278.

Weaver, A.M., Page, J.M., Guelcher, S.A., and Parekh, A. (2013). Synthetic and tissue-derived models for studying rigidity effects on invadopodia activity. Methods Mol. Biol. *1046*, 171–189.

Yamauchi, K., Yang, M., Jiang, P., Xu, M., Yamamoto, N., Tsuchiya, H., Tomita, K., Moossa, A.R., Bouvet, M., and Hoffman, R.M. (2006). Development of real-time subcellular dynamic multicolor imaging of cancer-cell trafficking in live mice with a variable-magnification whole-mouse imaging system. Cancer Res. *66*, 4208–4214.

Zijlstra, A., Lewis, J., Degryse, B., Stuhlmann, H., and Quigley, J.P. (2008). The inhibition of tumor cell intravasation and subsequent metastasis via regulation of in vivo tumor cell motility by the tetraspanin CD151. Cancer Cell *13*, 221–234.